# MAGNETIC FIELD SUPPRESSION OF MELT FLOW IN CRYSTAL GROWTH

Brian H. Dennis and George S. Dulikravich
Department of Mechanical and Aerospace Engineering, UTA Box 19018
The University of Texas at Arlington, Arlington, Texas 76019, USA

ABSTRACT. A least-squares spectral finite element method was used to develop an accurate computer code for prediction of solidification from a melt under the influence of an externally applied magnetic field. The computational results indicate significantly different flow-field patterns and thermal fields in the melt and the accrued solid in the cases of full gravity, reduced gravity, and an applied uniform magnetic field. This clearly suggests the possibility of optimizing magnetic field distribution and crucible shapes for controlling the melt recirculation.

## INTRODUCTION

When growing a crystal, such as a semiconductor crystal, it is desirable to remove the thermally induced convection effects entirely, leading to heat transfer by pure conduction. This is good for two reasons. First, if the velocity within the melt region is high, it is more likely that small particles of the crucible wall will be deposited in the crystal. Such contamination dramatically reduces the quality of the solid crystal. Second, for some semiconductors, a dopant is introduced into the melt. It is desirable to achieve a distribution of the dopant in the solid crystal that is as uniform as possible [1]. This is easier to realize under pure heat conduction with no convection [1]. One way to reduce the convection in the melt region is to perform the crystal growth in a low gravity environment, such as in an Earth-orbiting vehicle. Since semiconductor melts are highly electrically conducting, a more practical approach is to use magnetic and electric fields to suppress the buoyancy induced flows [2,3]. With such an electromagnetic device, high quality crystals can be produced under full gravity. Magnetic fields can be used to damp the convection during the directional solidification of electrically conductive melts [4,5]. Computational methods are needed to enhance our understanding of the phenomena occurring during the solidification of semiconductor melts. Effects like the bending of isomagnetic lines and the effects of different crucible shapes on the melt flow are difficult to model analytically and so they may be studied numerically. In addition, numerical simulation can be used together with optimization to determine the distributions of the magnetic field lines and the shape of the crucible that will minimize the convective flow throughout the melt.

In this paper, the growth of a silicon crystal under an applied magnetic field has been simulated with the p-version of the least-squares finite element method (LSFEM) [6,7,8] for magnetohydrodynamics (MHD) [9,10,11,12,13]. The solidification is modeled by using temperature dependent properties. The material properties for silicon are given in Table 1. Here, L is the latent heat of liquid/solid phase change. The subscripts $\ell$ and s refer to the liquid and solid properties, respectively.

In the mushy region (where $T_\ell > T > T_s$), the density, specific heat, latent heat, and the viscosity were taken as linear functions of temperature.

$$
\begin{aligned}
f &= \frac{T - T_s}{T_\ell - T_s} \\
\rho &= f\rho_\ell + (1-f)\rho_s \\
\eta &= f\eta_\ell + (1-f)\eta_s \\
C_p &= fC_{p\ell} + (1-f)C_{ps}
\end{aligned}
\qquad (1)
$$

Table 1
Parameters for MHD silicon crystal growth

| | | |
|---|---|---|
| Density of the melt | $\rho_\ell$ (kg m$^{-3}$) | 2550.0 |
| Density of the solid | $\rho_s$ (kg m$^{-3}$) | 2330.0 |
| Length of the container | Length (m) | 0.1 |
| Heat conductivity of the melt | $k_\ell$ (W kg$^{-1}$ K$^{-1}$) | 64.0 |
| Heat conductivity of the solid | $k_s$ (W kg$^{-1}$ K$^{-1}$) | 22.0 |
| Liquidus temperature | $T_\ell$ (K) | 1685.0 |
| Solidus temperature | $T_s$ (K) | 1681.0 |
| Specific heat of the melt | $C_{p\ell}$ (J kg$^{-1}$ K$^{-1}$) | 1059.0 |
| Specific heat of the solid | $C_{ps}$ (J kg$^{-1}$ K$^{-1}$) | 1038.0 |
| Viscosity of the melt | $\eta$ (kg m$^{-1}$ s$^{-1}$) | 0.0007 |
| Electric conductivity | $\sigma$ ($\Omega^{-1}$ m$^{-1}$) | 4.3 x 10$^4$ |
| Latent heat of phase change | L (J kg$^{-1}$) | 1.8 x 10$^6$ |
| Thermal expansion coefficient | $\beta$ (K$^{-1}$) | 1.4 x 10$^{-4}$ |

The solid regions are modeled as a melt with an extremely high viscosity $\eta_s = 10^3$ kg m$^{-1}$ s$^{-1}$ [2]. Consequently, the computed velocities in the solid regions are not identically zero, but are extremely small compared to the velocities in the melt. This formulation allows one code to simultaneously simulate heat transfer through solid, melt, and mushy regions. The effect of the latent heat, L, is included by using an enthalpy method [14]. Typically, the effect of the latent heat can be included in a numerical simulation by allowing a rapid variation in the heat capacity in the mushy region. This direct evaluation leads to satisfactory numerical integrations only if the curve of the heat capacity against the temperature does not possess sharp peaks. If the mushy region is completely contained within a single element, there is a chance that it may not fall on an integration point and hence the latent heat will not be accounted for in the integration process. A better approach is to work with enthalpy, H, which is a smooth function even in the phase change zone. The relation

$$
\rho C_p = \frac{dH}{dT} \qquad (2)
$$

is approximated by

$$
\rho C_p \approx \frac{\sqrt{(\partial H/\partial x)^2 + (\partial H/\partial y)^2}}{\sqrt{(\partial T/\partial x)^2 + (\partial T/\partial y)^2}} \qquad (3)
$$

in an attempt to avoid the possibility of missing the peak values $\rho C_p$ during the numerical integration.

## NUMERICAL METHODOLOGY

Both h- and p-type finite elements were implemented in this work. Details have been published recently by the authors [8,12,13,15]. The p-type finite elements were developed using hierarchical basis functions based on Jacobi polynomials. The hierarchical basis leads to a linear algebraic system with a natural multilevel structure that is well suited to adaptive enrichment. The sparse linear systems were solved by either direct sparse LU factorization or by iterative methods. Two iterative methods were implemented in the software, one based on a Jacobi preconditioned conjugate gradient and the another based a multigrid-like technique that uses the hierarchy of basis functions instead of a hierarchy of finer grids. The method was implemented in an object-oriented fashion using the C++ programming language. The software has been tested against analytic solutions and experimental data for Navier-Stokes equations and for channel flows through transverse electric and magnetic fields, for shear-driven cavity flows, buoyancy-driven cavity flows, and flow over a backward-facing step [13].

## NUMERICAL RESULTS

The solidification of a silicon crystal in a square container both with and without an applied magnetic field has been simulated. The container sides have the length of 0.1 m. The solidification occurs on the top wall of the container. The side walls are thermally insulated. A parabolic temperature profile is applied to the bottom of the container to simulate non-uniform heating of the melt. The temperature at the center of the bottom wall is 1688.0 K and the temperature at the bottom corners is set to 1686.0 K. A uniform temperature of 1676.0 K is applied to the top wall. A no-slip condition for velocity is enforced on all walls of the container. A quadrilateral mesh with 121 elements with a p-level of P = 6 is used for all cases. The computational mesh is shown in Figure 1. A uniform vertical magnetic field is applied to container by placing magnets on the top and bottom walls and using a perfect conductor on the side walls. Three distinct cases have been simulated. In all cases gravity acts in the vertical direction and is therefore aligned with the externally applied uniform magnetic field.

Table 2
The relevant dimensional and non-dimensional parameters for the three test cases

| Test case | Gravity $g\,(m\,s^{-2})$ | Magnetic field $B_o\,(T)$ | Reynolds no | Peclet no. | Rayleigh no. | Prandtl no. | Hartmann no. |
|---|---|---|---|---|---|---|---|
| 1 | 9.81 | 0.0 | 4269.14 | 49.4487 | 211103 | 0.0115828 | 0.0 |
| 2 | 0.1 | 0.0 | 431.029 | 4.99252 | 2151.92 | 0.0115828 | 0.0 |
| 3 | 9.81 | 1.0 | 4269.14 | 49.4487 | 211103.0 | 0.0115828 | 783.764 |

Figure 2a shows the computed streamlines within the melt region for case no. 1. A number of strong counter rotating vortices are present within the melt region. Figure 2b shows the computed velocity magnitude within the melt region. The maximum velocity is 0.0021 $m\,s^{-1}$ and occurs around x = 0.05 m and y = 0.015 m. The computed temperature distribution is shown in Figure 2c. The motion of the melt results in a temperature distribution that is different from that obtained under pure diffusion.

The second case uses reduced gravity that would exist if the crystal were grown in a very low Earth-orbiting massive space station. Figure 3a shows the resulting streamlines within the melt region. Two pairs of counter rotating vortices are present within the melt region. In this case, the vortices are weaker than in the first cases. Figure 3b shows the computed velocity magnitude within the melt region. The maximum velocity is 0.000172 $m\,s^{-1}$ and occurs around x = 0.05 m and y = 0.015 m. The computed temperature distribution is shown in Figure 3c. The temperature distribution is very similar to that obtained under pure diffusion.

The third case uses full gravity with an applied magnetic field strength of 1.0 Tesla. Figure 4a shows the resulting streamlines within the melt region. Only one pair of counter rotating vortices are present within the melt region. The magnetic field has completely suppressed the secondary vortices that were present in the cases without the magnetic field. Figure 4b shows the computed velocity magnitude within the melt region. The maximum velocity is 0.0000434 $m\,s^{-1}$ and occurs around x = 0.05 m and y = 0.018 m. The computed temperature distribution is shown in Figure 4c. The temperature distribution is very similar to that obtained under pure diffusion. This case demonstrates that buoyancy induced flow velocities can be significantly reduced through the use of applied magnetic fields.

It should be noted that in this analysis it is assumed that the solid and the liquid regions have the same electrical conductivity. In the real case, the electrical conductivity may vary significantly between the solid and liquid phases. This change in conductivity would result in the bending of the magnetic field lines though the mushy region [4]. The present LSFEM algorithm would need to be modified to include a front tracking algorithm in order to accurately account for this effect.

## CONCLUSIONS AND RECOMMENDATIONS

Although the magnetic field significantly reduces the velocity of the flow within the melt, the crystal may still be slightly contaminated. It is desirable to completely eliminate the motion within the melt. It is possible that a uniform magnetic field much stronger than 1.0 Tesla may be required. Such magnets require superconducting ceramics and are costly to maintain. It may be possible to use the current LSFEM based software for combined electro-magneto-hydrodynamics (EMHD) [11,12] together with numerical optimization software to optimize the shape of the container as well as the distribution of the magnetic field along the container wall [15] that may locally eliminate the motion in the melt with lower strength magnets.

## REFERENCES


1. Hirtz, J. M. and Ma, N., Dopant Transport During Semiconductor Crystal Growth: Axial versus Transverse Magnetic Field, *J. of Crystal Growth*, Vol. 210, pp. 554-572, 2000.

2. Dulikravich, G. S., Ahuja, V. and Lee, S., Modeling Three-Dimensional Solidification With Magnetic Fields and Reduced Gravity, *International Journal of Heat and Mass Transfer*, Vol. 37, No. 5, pp. 837-853, 1994.

3. Dulikravich, G. S., Choi, K. - Y. and Lee, S., Magnetic Field Control of Vorticity in Steady Incompressible Laminar Flows, *Symposium on Developments in Electrorheological Flows and Measurement Uncertainty* 1994, ASME WAM'94, (eds.: D. A. Siginer, J. H. Kim, S. A. Sheriff and H. W. Colleman), Chicago, IL, Nov. 6-11, 1994, ASME FED-Vol. 205/AMD-Vol. 190, pp. 125-142, 1994.

4. Fedoseyev, K. I., Kansa, E. J., Marin, C. and Ostrogorsky, A. G., Magnetic Field Suppression of Semiconductor Melt Flow in Crystal Growth: Comparison of Three Methods for Numerical Modeling, *CFD Journal*, 2000.

5. Meir, A. J., Schmidt, P. G., Bakhtiyarov, S. I. and Overfelt, R. A., Velocity, Potential, and Temperature Distributions in Molten Metals During Electromagnetic Stirring, Part II: Numerical Simulations. Symp. on Rheology and Fluid Mechanics of Nonlinear Materials, ASME IMECE'99, (ed: D. A. Siginer), Nashville, TN, Nov. 14-19, 1999, ASME FED-Vol. 249, pp. 97-104, 1999.

6. Botchev, P. B., Analysis of Least-Squares Finite Element Methods for Navier-Stokes Equations, *SIAM J. of Numerical Analysis*, Vol. 34, No. 5, pp. 1817-1844, 1997.
7. Jiang, B.-N., *The Least-Squares Finite Element Method*, Springer-Verlag, Berlin, 1998.

8. Dennis, B. H. and Dulikravich, G. S., Simulation of Magnetohydrodynamics With Conjugate Heat Transfer, ECCOMAS 2000, *Proc. of European Congress on Computational Methods in Applied Sciences and Engineering*, (ed.: Onate, E.), September 11-14, 2000, Barcelona, Spain.

9. Dulikravich, G. S. and Lynn, S. R., Unified Electro-Magneto-Fluid Dynamics (EMFD): A Survey of Mathematical Models, *Internat. J. of Non-Linear Mechanics*, Vol. 32, No. 5, September 1997, pp. 923-932.

10. Dulikravich, G. S., Electro-Magneto-Hydrodynamics and Solidification, Chapter no. 9 in *Advances in Flow and Rheology of Non-Newtonian Fluids, Part B* (eds: D. A. Siginer, D. De Kee and R. P. Chhabra), Rheology Series, 8, Elsevier Publishers, June 1999, pp. 677-716.

11. Ko, H.-J. and Dulikravich, G. S., A Fully Non-Linear Model of Electro-Magneto-Hydrodynamics, Symposium on Rheology and Fluid Mechanics of Non-Linear Materials, (eds.: D. A. Siginer and D. De Kee), Anaheim, CA, Nov. 15-20, 1998, ASME FED-Vol. 246/MD-Vol. 81, pp. 173-182; also in *Internat. J. of Non-Linear Mechanics*, Vol. 35, No. 4, 2000, pp. 709-719.

12. Dennis, B. H. and Dulikravich, G. S., Electromagnetohydrodynamics (EMHD): Numerical Experiments in Planar Steady Flows, *Symposium on Recent Advances in the Mechanics of Structured Continua*, (eds: Massoudi, M. and Rajagopal, K. R.), ASME IMECE 2K, Orlando, FL, November 5-10, 2000, AMD-Vol. 244/MD-Vol. 92, pp. 17-24.

13. Dennis, B. H., Simulation and Optimization of Electromagnetohydrodynamic Flows, *Ph.D. Thesis*, Aerospace Eng. Dept., Pennsylvania State University, University Park, PA, Dec. 2000.

14. Morgan, K., Lewis, R. W. and Zienkiewicz, O. C., An Improved Algorithm for Heat Conduction and Problems with Phase Change, *Internat. J. for Numerical Methods in Engineering*, pp. 1191-1195, 1977.

15. Dennis, B. H. and Dulikravich, G. S., Optimization of Magneto-Hydrodynamic Control of Diffuser Flows Using Micro-Genetic Algorithm and Least Squares Finite Elements, *J. of Finite Elements in Analysis and Design*, December 2000.

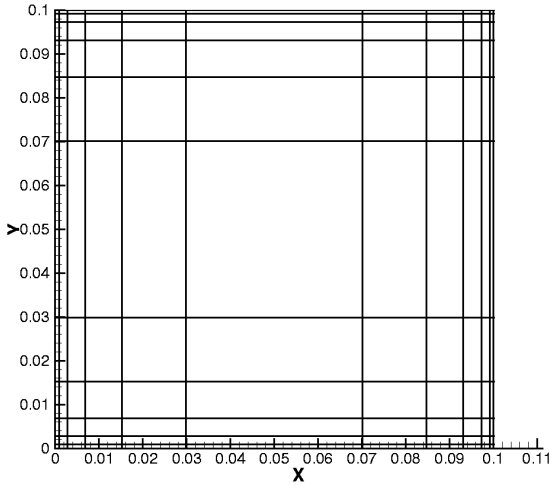


Figure 1. Computational grid used in the p-version LSFEM

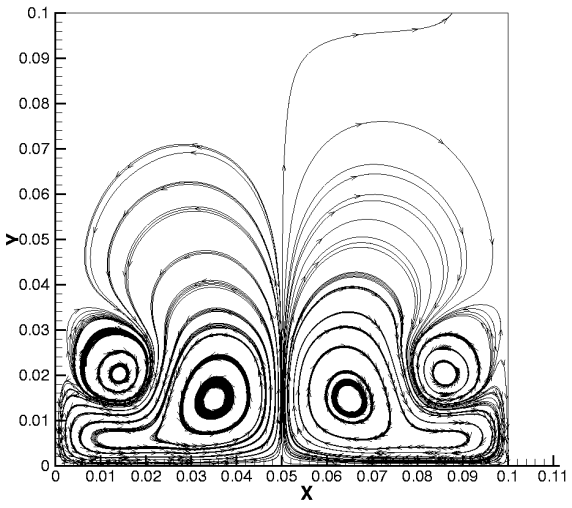


a)

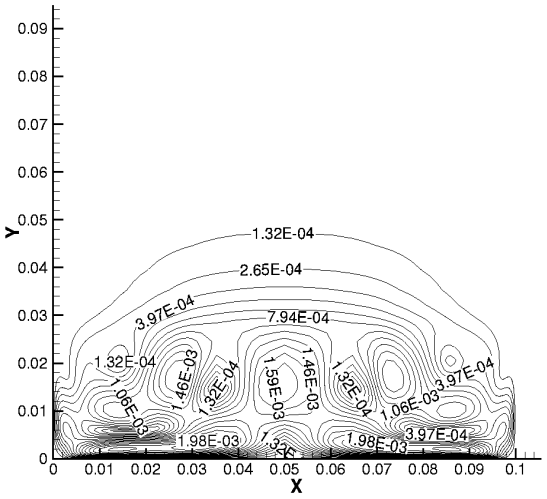


b)

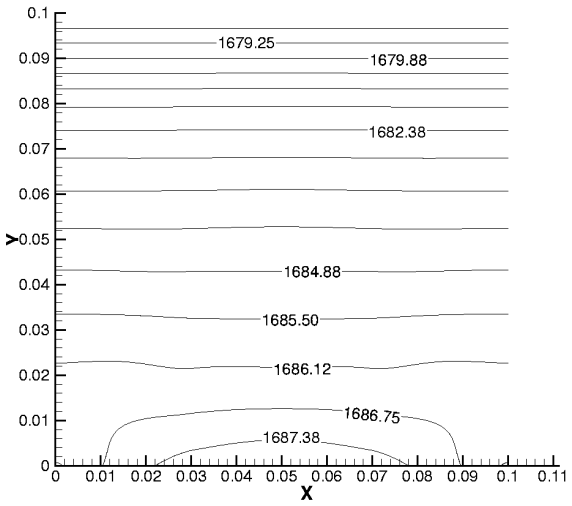


c)

Figure 2. Results for test case no. 1 (full gravity and no magnetic field); a) streamlines, b) velocity magnitudes, c) isotherms.

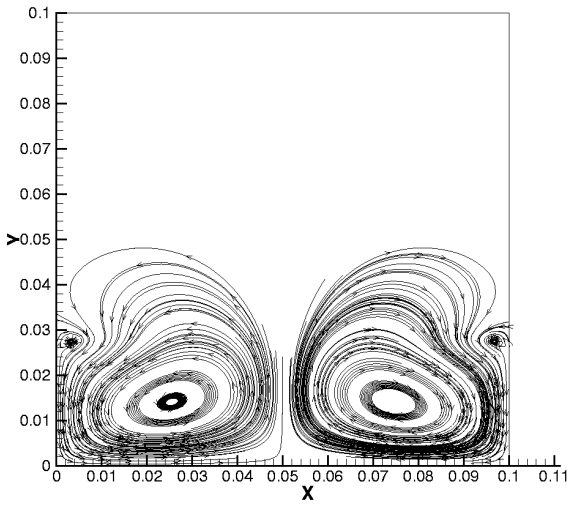


a)

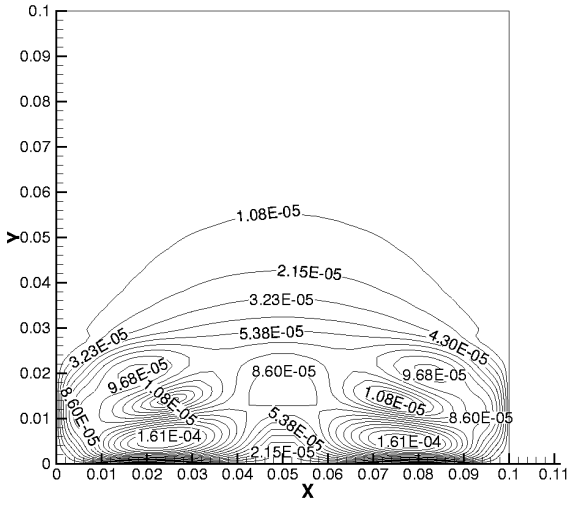


b)

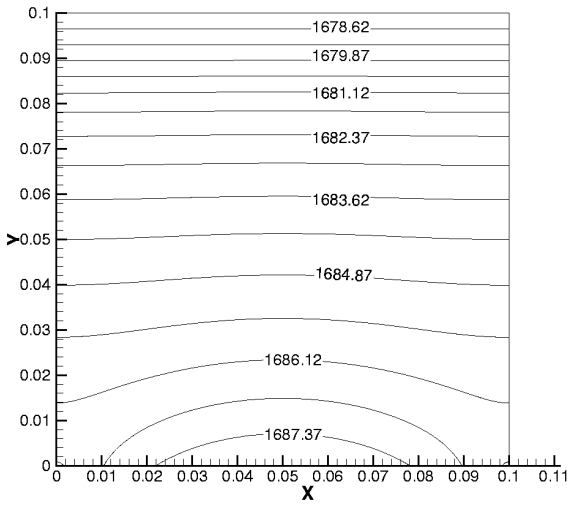


c)

Figure 3. Results for test case no. 2 (reduced gravity and no magnetic field); a) streamlines, b) velocity magnitudes, c) isotherms.

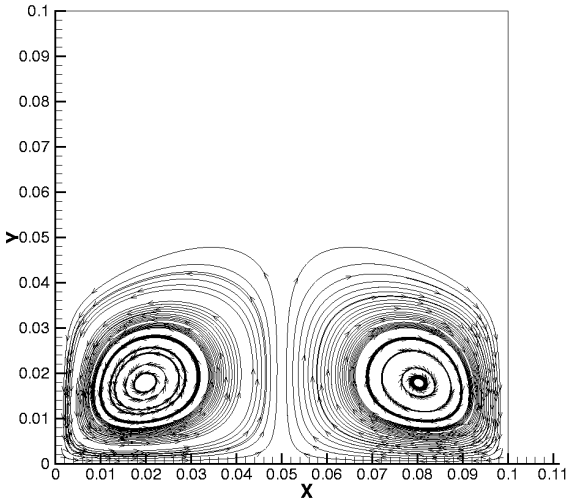


a)

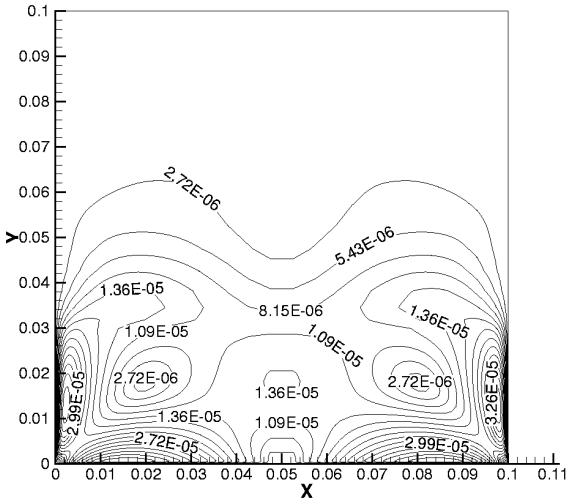


b)

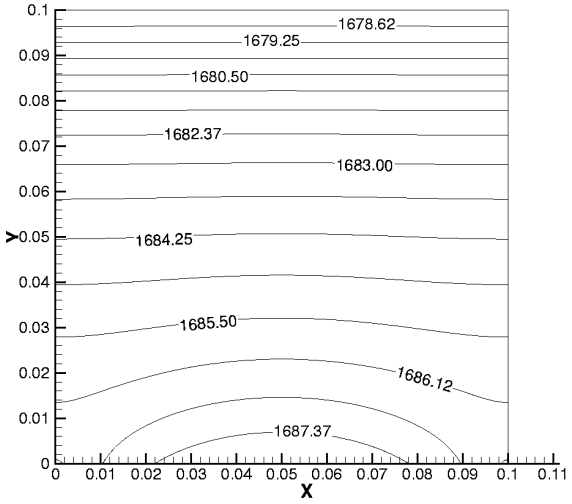


c)

Figure 4. Results for test case no. 3 (full gravity and 1 T magnetic field); a) streamlines, b) velocity magnitudes, c) isotherms.